

Theory of tunneling spectroscopy of normal metal/ferromagnet/spin-triplet superconductor junctions

L.A.B. Olde Olthof¹, S.-I. Suzuki², A.A. Golubov^{1,3}, M. Kunieda⁴, S. Yonezawa⁴, Y. Maeno⁴, and Y. Tanaka²

¹MESA⁺ Institute for Nanotechnology, University of Twente, The Netherlands

²Department of Applied Physics, Nagoya University, Nagoya, 464-8603, Japan

³Moscow Institute of Physics and Technology, Dolgoprudny, Moscow Region, 141700, Russia and

⁴Department of Physics, Graduate School of Science, Kyoto University, Kyoto 606-8502, Japan

We study the tunneling conductance of a ballistic normal metal / ferromagnet / spin-triplet superconductor junction using the extended Blonder-Tinkham-Klapwijk formalism as a model for a c -axis oriented Au / SrRuO₃ / Sr₂RuO₄ junction. We compare chiral p -wave (CPW) and helical p -wave (HPW) pair potentials, combined with ferromagnet magnetization directions parallel and perpendicular to the interface. For fixed θ_M , where θ_M is a direction of magnetization in the ferromagnet measured from the c -axis, the tunneling conductance of CPW and HPW clearly show different voltage dependencies. It is found that the cases where the d -vector is perpendicular to the magnetization direction (CPW with $\theta_M = \pi/2$ and HPW with $\theta_M = 0$) are identical. The obtained results serve as a guide to determine the pairing symmetry of the spin-triplet superconductor Sr₂RuO₄.

I. INTRODUCTION

Nowadays, Sr₂RuO₄ is known as an unconventional superconductor with the transition temperature $T_c \sim 1.5$ K.¹ The fact that the Knight shift does not change across T_c is consistent with spin-triplet pairing.²⁻⁶ Various theoretical studies have discussed the microscopic mechanism of spin-triplet pairings in this material.⁷⁻²¹ The existence of a zero bias conductance peak in several tunneling experiments^{22,23} indicates the realization of unconventional superconductivity.²⁴⁻²⁶ In particular, the broad zero bias conductance peak observed in tunneling spectroscopy suggests the realization of a surface Andreev bound states (SABS) with linear dispersion²⁶⁻²⁹. This is in contrast with high T_c cuprate superconductors, where a sharp zero bias conductance peak is observed^{24,25,30-35} due to flat band zero energy states.^{24,36,37} When spin-triplet pairing is realized, we can expect exotic phenomena, such as the so called anomalous proximity effect in diffusive normal metal / spin-triplet superconductor junctions.³⁸⁻⁴²

The presence or absence of time reversal symmetry (TRS) in Sr₂RuO₄ is an important issue. Among two-dimensional spin-triplet p -wave pairings, chiral and helical p -wave pairing seem promising in the absence and presence of TRS, respectively.⁴³ Broken TRS was observed in μ SR and Kerr-rotation experiments as a result of a spontaneous internal magnetic field below T_c ,⁴⁴⁻⁴⁷ which supports chiral p -wave pairing. However, the internal magnetic field has not been detected in scanning SQUID experiments,^{48,49} which suggests realization of helical p -wave symmetry. Although there are several possible explanations for the absence of broken TRS in Sr₂RuO₄,^{17,50-56} the pairing symmetry remains a point of discussion. One of the main differences between these two pairing symmetries is the direction of d -vector.

A constructive way to distinguish between them is to study the charge transport in ferromagnet / spin-triplet

superconductor junctions.⁵⁷⁻⁶¹ Naively speaking, the direction of the magnetization axis with respect to the d -vector (parallel or perpendicular) influences the charge transport. Recently, a Au / SrRuO₃ / Sr₂RuO₄ junction oriented along the c -axis has been fabricated by means of epitaxial growth.⁶² Since SrRuO₃ and Sr₂RuO₄ have similar a -axis lattice constants, as well as similar atomic arrangements, a smooth interface between them can be expected, which turns this system into a nice playground for clarifying the direction of the d -vector. Because the SABS is absent in this direction, we can directly compare the effect of the magnetization direction relative to the d -vector. To interpret the experimental results, a theoretical model is required in which we calculate the tunneling conductance along the c -axis, based on a minimal model which takes the quasi-two dimensional nature of Sr₂RuO₄ into account.

In this paper, we investigate normal metal (N) / ferromagnet (F) / spin-triplet superconductor (S) junctions with s -wave, chiral and helical p -wave pairing symmetries by changing the properties of the ferromagnet, *e.g.*, thickness, magnetization strength and direction. The anisotropic Fermi surface of Sr₂RuO₄ and realistic effective masses are also included, since the Fermi-momentum mismatch changes the transparency and the resulting conductance. Finally, an external magnetic field is taken into account through the Doppler shift.

II. FORMULATION

A. Model and Hamiltonian

We consider a three-dimensional N/F/S junction, as shown in Fig. 1. We assume the junction interfaces to be perpendicular to the z -axis and located at $z = 0$ and $z = L$. The F has a thickness L and a magnetization $\mathbf{M}(z)$. The N and S are considered to be semi-

infinite. Superconducting junctions are described by the Bogoliubov-de Gennes (BdG) Hamiltonian

$$\check{H}(\mathbf{r}) = \begin{bmatrix} \hat{h}(\mathbf{r}, H) & \hat{\Delta}(\mathbf{r}) \\ -\hat{\Delta}^*(\mathbf{r}) & -\hat{h}^*(\mathbf{r}, H) \end{bmatrix}, \quad (1)$$

where the basis is taken as $\Psi(\mathbf{r}) = [\psi_\uparrow(\mathbf{r}) \ \psi_\downarrow(\mathbf{r}) \ \psi_\uparrow^\dagger(\mathbf{r}) \ \psi_\downarrow^\dagger(\mathbf{r})]^T$, where T is the transpose, the symbol $\hat{(\cdot)}$ represents a 2×2 (4×4) matrix in the spin (spin-Nambu) space, H is an externally applied magnetic field in the x -direction. Since the system has translational symmetry in the x - and y -direction, the momenta k_x and k_y are well-defined quantum numbers. Therefore, the wave function can be expressed in the Fourier components as

$$\Psi(\mathbf{r}) = \sum_{\mathbf{k}_\parallel} \Psi_{\mathbf{k}_\parallel}(z) \frac{e^{i(k_x x + k_y y)}}{\sqrt{L_x L_y}}, \quad (2)$$

$$\Psi_{\mathbf{k}_\parallel}(z) = [\psi_{\uparrow, \mathbf{k}_\parallel} \ \psi_{\downarrow, \mathbf{k}_\parallel} \ \psi_{\uparrow, -\mathbf{k}_\parallel}^\dagger \ \psi_{\downarrow, -\mathbf{k}_\parallel}^\dagger]^T, \quad (3)$$

where $\mathbf{k}_\parallel = (k_x, k_y, 0)$. In Eq. (2), we assume periodic boundary conditions in order to accommodate the infinite dimensions in the x - and y -direction. The lateral dimensions L_x and L_y are normalization factors and do not affect the conductance spectrum. The Hamiltonian becomes

$$\check{H}_{\mathbf{k}_\parallel}(z, H) = \begin{bmatrix} \hat{h}_{\mathbf{k}_\parallel}(z, H) & \hat{\Delta}_{\mathbf{k}_\parallel}(z) \\ -\hat{\Delta}_{-\mathbf{k}_\parallel}^*(z) & -\hat{h}_{-\mathbf{k}_\parallel}^*(z, H) \end{bmatrix}. \quad (4)$$

The single-particle Hamiltonian $\hat{h}_{\mathbf{k}_\parallel}$ is given by

$$\hat{h}_{\mathbf{k}_\parallel}(z, H) = \xi_{\mathbf{k}_\parallel}(z, H) + \mathbf{M}(z) \cdot \hat{\boldsymbol{\sigma}} + \hat{F}_{\mathbf{k}_\parallel}(z), \quad (5)$$

$$\xi_{\mathbf{k}_\parallel}(z, H) = -\frac{\hbar^2}{2m_z} \frac{\partial^2}{\partial z^2} - \mu' - \Delta_0 \frac{H}{H_c} \frac{k_\parallel}{k_F} \sin \varphi, \quad (6)$$

$$\mu' = \mu - \frac{\hbar^2}{2} \left[\frac{k_x^2}{m_x} + \frac{k_y^2}{m_y} \right], \quad (7)$$

where $\xi_{\mathbf{k}}$ is the kinetic energy in the presence of an external magnetic field in the x -direction and μ is the chemical potential, which we assume to be constant across the

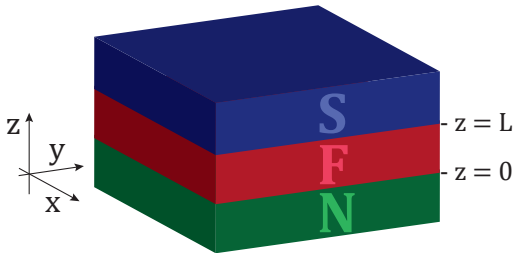


FIG. 1. Schematic of the three-dimensional normal metal(N)/ferromagnet(F)/superconductor(S) junction. We assume the structure extends to infinity in all directions.

junction. A full derivation of Eq. (6) is given in Appendix A. The matrices $\hat{\sigma}_j$ ($j \in \{x, y, z\}$) and $\hat{\sigma}_0$ are the Pauli matrices and the identity matrix in spin space, $\hat{\boldsymbol{\sigma}} = \hat{\sigma}_x \mathbf{e}_x + \hat{\sigma}_y \mathbf{e}_y + \hat{\sigma}_z \mathbf{e}_z$ with \mathbf{e}_j being the unit vectors in the j -direction. We can modify the shape of Fermi surfaces by tuning the effective masses $\mathbf{m} = (m_x, m_y, m_z)$ in each region. In this paper, we parametrize \mathbf{m} as

$$\mathbf{m}(z) = \begin{cases} (m_N, m_N, m_N) & \text{for } z \leq 0, \\ (m_F, m_F, m_F) & \text{for } 0 < z < L, \\ (m_\parallel, m_\parallel, m_\perp) & \text{for } z \geq L. \end{cases} \quad (8)$$

The magnetization is described as⁶¹

$$\mathbf{M}(z) = M_0(\sin \theta_M \mathbf{e}_x + \cos \theta_M \mathbf{e}_z) \Theta(z) \Theta(L - z), \quad (9)$$

where $\Theta(z)$ is the Heaviside step function. In this paper, we ignore the re-orientation of the d -vector by the magnetization in F⁶³⁻⁶⁶ for simplicity. The effects of the interfaces are described by $\hat{F}_{\mathbf{k}_\parallel}(z)$ as⁶⁷

$$\hat{F}_{\mathbf{k}_\parallel}(z) = \delta(z) \hat{F}_1 + \delta(z - L) \hat{F}_2, \quad (10)$$

$$\hat{F}_{1, \mathbf{k}_\parallel} = F_1 \hat{\sigma}_0, \quad (11)$$

$$\hat{F}_{2, \mathbf{k}_\parallel} = F_{\text{SO}} \mathbf{e}_z \cdot (\hat{\boldsymbol{\sigma}} \times \mathbf{k}), \quad (12)$$

where F_1 and F_{SO} represent the strengths of the barrier potential at $z = 0$ and the spin-orbit coupling (SOC) at $z = L$, respectively. The SOC term reduces to

$$\mathbf{e}_z \cdot (\hat{\boldsymbol{\sigma}} \times \mathbf{k}) = \hat{\sigma}_x k_y - \hat{\sigma}_y k_x \quad (13)$$

$$= ik_\parallel \begin{bmatrix} 0 & e^{-i\varphi} \\ -e^{+i\varphi} & 0 \end{bmatrix}, \quad (14)$$

where $k_x = k_\parallel \cos \varphi$ and $k_y = k_\parallel \sin \varphi$ with $k_\parallel = (k_x^2 + k_y^2)^{1/2}$. The pair potential is described by

$$\hat{\Delta}_{\mathbf{k}_\parallel}(z) = \hat{\Delta}_{\mathbf{k}_\parallel}(z) \Theta(z - L). \quad (15)$$

The momentum dependence of the pair potentials for s -wave (SW), chiral p -wave (CPW), and helical p -wave (HPW) superconductors are written as

$$\hat{\Delta}_{\mathbf{k}_\parallel}(z) = \begin{cases} \Delta_0 i \hat{\sigma}_y & \text{for SW,} \\ \Delta_0 [\bar{k}_x + i \chi \bar{k}_y] \hat{\sigma}_x & \text{for CPW,} \\ \Delta_0 [\bar{k}_x \hat{\sigma}_0 + i \bar{k}_y \hat{\sigma}_z] & \text{for HPW,} \end{cases} \quad (16)$$

where Δ_0 is a constant which characterizes the amplitude of the pair potential, χ is so-called the chirality (which can be ± 1), $\bar{k}_x = k_x/k_{s\parallel}$ with $k_{s\parallel} = \sqrt{2m_\parallel \mu'}/\hbar$ being the Fermi wavenumber in k_x - k_y plane for S. The assumption that Δ_0 is constant implies that we do not take the inverse proximity effect (from F into S) into account, which is a common assumption.⁶⁸

B. Wave functions

The wave function is obtained by solving the Hamiltonian at an energy E in each region. Throughout this paper, we assume $E \sim \Delta_0 \ll \mu$. The wave function for $z \leq 0$ is given by

$$\Psi_{\mathbf{k}_\parallel}(z) = \check{K}_N^+ \vec{i} + \check{K}_N^- \vec{r}, \quad (17)$$

where $\check{K}_N^\pm = e^{\pm i \tilde{\tau}_z k_N z}$ with $k_N = \sqrt{2m_N \mu'} / \hbar$ and $\tilde{\tau}_z = \text{diag}[\hat{\sigma}_0, -\hat{\sigma}_0]$ being the third Pauli matrix in Nambu space. The vector \vec{i} represents the wave function amplitude of the incident particles which is given by

$$\vec{i} = \begin{cases} [1 \ 0 \ 0 \ 0]^T & \text{for an up-spin electron,} \\ [0 \ 1 \ 0 \ 0]^T & \text{for a down-spin electron.} \end{cases} \quad (18)$$

The vector \vec{r} describes the wave function amplitude of the reflected particles as

$$\vec{r} = [r_\uparrow^p \ r_\downarrow^p \ r_\uparrow^h \ r_\downarrow^h]^T, \quad (19)$$

where r_α^p and r_α^h , $\alpha \in \{\uparrow, \downarrow\}$ are the normal and Andreev reflection coefficients, respectively. The wave function for $0 < z < L$ is given by

$$\Psi_{\mathbf{k}_\parallel}(z) = \check{A} \check{K}_F^+ \vec{f}_P + \check{A} \check{K}_F^- \vec{f}_N, \quad (20)$$

where $\check{K}_F^\pm = \text{diag}[e^{\pm i k_F^+ z}, e^{\pm i k_F^- z}, e^{\pm i k_F^+ z}, e^{\pm i k_F^- z}]$ with $k_F^\pm = \sqrt{2m_F(\mu' \mp M_0)} / \hbar$. The matrix $\check{A} = \text{diag}[\hat{A}, \hat{A}]$ characterizes the spin structure of the F, where \hat{A} is given by⁶¹

$$\hat{A} = \begin{bmatrix} \cos(\theta_M/2) & -\sin(\theta_M/2) \\ \sin(\theta_M/2) & \cos(\theta_M/2) \end{bmatrix} \quad (21)$$

The vectors $\vec{f}_{P(N)}$ describe the wave function amplitudes of particles propagating in the positive (negative) z -direction. They are defined as

$$\vec{f}_P = [f_{\uparrow,P}^p \ f_{\downarrow,P}^p \ f_{\uparrow,P}^h \ f_{\downarrow,P}^h]^T, \quad (22)$$

$$\vec{f}_N = [f_{\uparrow,N}^p \ f_{\downarrow,N}^p \ f_{\uparrow,N}^h \ f_{\downarrow,N}^h]^T. \quad (23)$$

The wave function for $z \geq L$ is given by

$$\Psi_{\mathbf{k}_\parallel}(z) = \check{U} \check{K}_S \vec{t}, \quad (24)$$

where $\check{K}_S = \text{diag}[e^{+i k_S z}, e^{+i k_S z}, e^{-i k_S z}, e^{-i k_S z}]$ with $k_S = \sqrt{2m_\perp \mu'} / \hbar$. The vector \vec{t} describes the wave function amplitudes of the transmitted particles as

$$\vec{t} = [t_\uparrow^p \ t_\downarrow^p \ t_\uparrow^h \ t_\downarrow^h]^T. \quad (25)$$

The matrix \check{U} describes the amplitude of the wave function in the superconductor as

$$\check{U} = \begin{bmatrix} u_{\mathbf{k}_\parallel} \hat{\sigma}_0 & v_{\mathbf{k}_\parallel} \hat{D}_{\mathbf{k}_\parallel} \\ v_{\mathbf{k}_\parallel} \hat{D}_{\mathbf{k}_\parallel}^\dagger & u_{\mathbf{k}_\parallel} \hat{\sigma}_0 \end{bmatrix}, \quad (26)$$

$$\hat{D}_{\mathbf{k}_\parallel} = \hat{\Delta}_{\mathbf{k}_\parallel} / \Delta_0, \quad (27)$$

with

$$u_{\mathbf{k}_\parallel} = \frac{1}{\sqrt{2}} \sqrt{1 + \frac{\Omega_{\mathbf{k}_\parallel}}{E}}, \quad (28)$$

$$v_{\mathbf{k}_\parallel} = \frac{1}{\sqrt{2}} \sqrt{1 - \frac{\Omega_{\mathbf{k}_\parallel}}{E}}, \quad (29)$$

$$\Omega_{\mathbf{k}_\parallel} = \sqrt{E^2 - |d_{\mathbf{k}_\parallel}|^2}, \quad (30)$$

where $d_{\mathbf{k}_\parallel}$ is obtained from the relation $d_{\mathbf{k}_\parallel} \hat{\sigma}_0 = \hat{\Delta}_{\mathbf{k}_\parallel} \hat{\Delta}_{\mathbf{k}_\parallel}^\dagger$.

C. Differential conductance

All coefficients in Eq. (17), (20) and (24) can be determined by the four boundary conditions at $z = 0$ and $z = L$. The first two boundary conditions are derived from continuity at $z = 0$. They are given by⁶⁸

$$\lim_{z \uparrow 0} \Psi_{\mathbf{k}_\parallel} = \lim_{z \downarrow 0} \Psi_{\mathbf{k}_\parallel}, \quad (31)$$

$$\lim_{z \uparrow 0} \left[\frac{\partial \Psi_{\mathbf{k}_\parallel}}{\partial z} + \frac{2m(z)}{\hbar^2} \check{F}_1 \Psi_{\mathbf{k}_\parallel} \right] = \lim_{z \downarrow 0} \frac{\partial \Psi_{\mathbf{k}_\parallel}}{\partial z}, \quad (32)$$

where $\check{F}_1 = \text{diag}[\hat{F}_{1,\mathbf{k}_\parallel}, -\hat{F}_{1,-\mathbf{k}_\parallel}^*]$. The other boundary conditions are related to the interface at $z = L$ as follows

$$\lim_{z \uparrow L} \Psi_{\mathbf{k}_\parallel} = \lim_{z \downarrow L} \Psi_{\mathbf{k}_\parallel}, \quad (33)$$

$$\lim_{z \uparrow L} \left[\frac{\partial \Psi_{\mathbf{k}_\parallel}}{\partial z} + \frac{2m(z)}{\hbar^2} \check{F}_2 \Psi_{\mathbf{k}_\parallel} \right] = \lim_{z \downarrow L} \frac{\partial \Psi_{\mathbf{k}_\parallel}}{\partial z}, \quad (34)$$

where $\check{F}_2 = \text{diag}[\hat{F}_{2,\mathbf{k}_\parallel}, -\hat{F}_{2,-\mathbf{k}_\parallel}^*]$.

In the supplemental material, we derived the expression for the current through the N/F/S junction and found that it was the same as in the original BTK theory.⁶⁸ Hence, we can use the same differential tunnelling conductance resulting from a spin- α incident particle, which is given by

$$\sigma(E) = \sum'_{\mathbf{k}_\parallel, \alpha} \sigma_\alpha(E, \mathbf{k}_\parallel), \quad (35)$$

$$\sigma_\alpha(E, \mathbf{k}_\parallel) = 1 + |r_\uparrow^h|^2 + |r_\downarrow^h|^2 - |r_\uparrow^p|^2 - |r_\downarrow^p|^2, \quad (36)$$

where $\sigma_\alpha(E, \mathbf{k}_\parallel)$ is the angle-resolved differential conductance for a spin- α incident particle with $\alpha \in \{\uparrow, \downarrow\}$.⁶⁹ To model a cylindrical Fermi surface in a quasi-two-dimensional material, we introduce a cutoff in the summation with respect to \mathbf{k}_\parallel as

$$\sum'_{\mathbf{k}_\parallel, \alpha} \dots \stackrel{\text{def}}{=} \sum_{\mathbf{k}_\parallel, \alpha} \dots \Theta(|\mathbf{k}_\parallel| - k_c) \quad (37)$$

where $k_c = k_N \sin \theta_c$ and θ_c is the cutoff angle.

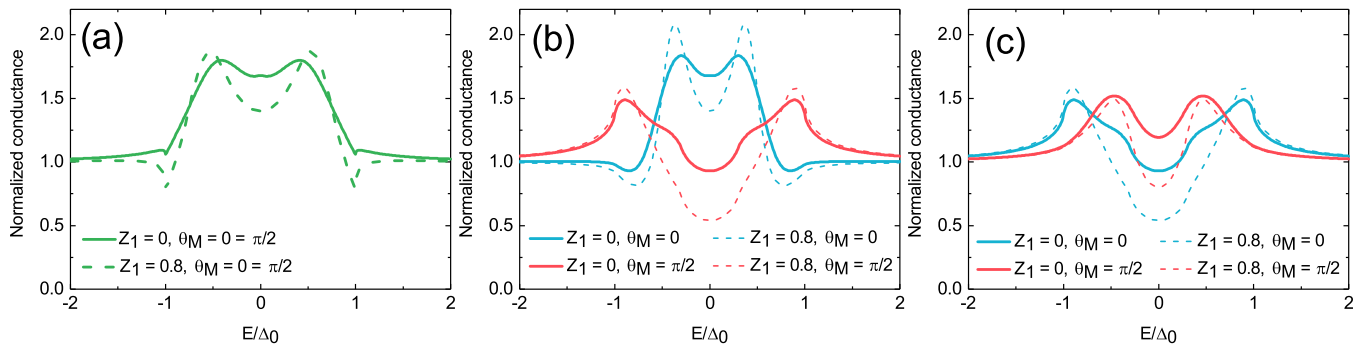


FIG. 2. The dimensionless tunneling conductance using pair potentials (a) SW, (b) CPW and (c) HPW. Without barriers ($Z_1 = 0$, solid graphs) and including a small barrier at the first interface ($Z_1 = 0.8$, dashed graphs). The SW case is independent of the magnetization angle. For CPW and HPW, the magnetization angle varies from $\theta_M = 0$ (blue graphs) to $\theta_M = \pi/2$ (red graphs). $X = 0.6$, $k_F L = 11$.

	s -wave	Chiral p -wave	Helical p -wave
$\mathbf{M} \parallel \mathbf{z}$	$\begin{bmatrix} & 1 \\ -1 & \end{bmatrix}$	$\begin{bmatrix} & e^{i\chi\phi} \\ e^{i\chi\phi} & \end{bmatrix}$	$\begin{bmatrix} e^{i\phi} & \\ & e^{-i\phi} \end{bmatrix}$
$\mathbf{M} \parallel \mathbf{x}$	$\begin{bmatrix} & 1 \\ -1 & \end{bmatrix}$	$\begin{bmatrix} e^{i\chi\phi} & \\ & -e^{i\chi\phi} \end{bmatrix}$	$\begin{bmatrix} \bar{k}_x & -i\bar{k}_y \\ -i\bar{k}_y & \bar{k}_x \end{bmatrix}$

TABLE I. Matrix structure of the pair potential. The spin-quantisation axis is taken to be parallel to the magnetisation vector \mathbf{M} . The first and second rows are for $\mathbf{M} \parallel \mathbf{z}$ (i.e., $\theta_M = 0$) and for $\mathbf{M} \parallel \mathbf{x}$ (i.e., $\theta_M = \pi/2$), respectively. From the table, we can see that the 4×4 Hamiltonian can be reduced to two 2×2 Hamiltonian matrices except for the helical p -wave with $\theta_M = \pi/2$ case. The angle ϕ satisfies the relations: $k_x = k_{\parallel} \cos \phi$ and $k_y = k_{\parallel} \sin \phi$ with $k_{\parallel} = |\mathbf{k}_{\parallel}|$ being the momentum parallel to the interfaces. The momentum is normalized: $\bar{k}_{x(y)} = k_{x(y)}/k_{\parallel}$. The factor χ is the chirality of a chiral p -wave superconductor.

III. RESULTS

The aim of this paper is to model the conductance of a Au/SrRuO₃/Sr₂RuO₄ junction. A realistic effective mass for ferromagnet SrRuO₃ is $m_F = 7m_N$.⁷⁰ We approximate the Sr₂RuO₄ γ -band by modelling the Fermi surface as an ellipsoid ($m_{\parallel} = 1.3$, $m_{\perp} = 16$) with its top and bottom cut off ($\theta_c = \pi/10$). We will compare a N/F/S junction without barriers to a N/F/S with a small tunnel barrier F_1 at the N/F interface. Because of epitaxial growth and minimal lattice mismatch, a smooth F/S interface is expected and therefore, no barrier is introduced. The spin-orbit coupling is set to zero in the main text of the main text. Effects of F_{SO} are discussed in Appendix C.

A. Direction of the magnetization

We first show the differential conductances of a junction with a spin-singlet s -wave superconductor in Fig. 2(a), where results with and without the interface barrier are indicated by solid and dashed lines, respec-

tively. Throughout this paper, the differential conductance is normalized by its value in the normal state (i.e., $\Delta_0 = 0$) and the energy is normalized by the maximum amplitude of the pair potential in the absence of an external magnetic field, Δ_0 . As shown in Fig. 2(a), the coherence peaks appear at an energy lower than the gap amplitude ($E \approx 0.6\Delta_0$) which is a result of the ferromagnet with finite thickness L . Comparing the solid and dashed lines, we see that the barrier potential at the N/F interface sharpens the peaks around $E \approx 0.5\Delta_0$ and the dips around $E \approx \Delta_0$ in the differential conductance. In addition, the zero-energy dip becomes more prominent with increasing barrier. This is consistent with the well-known N/S junction.⁶⁸ In spin-singlet superconductors the conductance does not depend on the direction of the magnetization (i.e., θ_M) because a singlet Cooper pair does not have a finite total spin. It should be noted that, throughout this paper, the pair potential is taken non-self-consistent (i.e., Δ_0 is constant). The sharp peaks in the conductance would be broadened and lowered if we would include the self-consistency.⁷¹

The differential conductance of the spin-triplet CPW and HPW superconductors are shown in Figs. 2(b) and

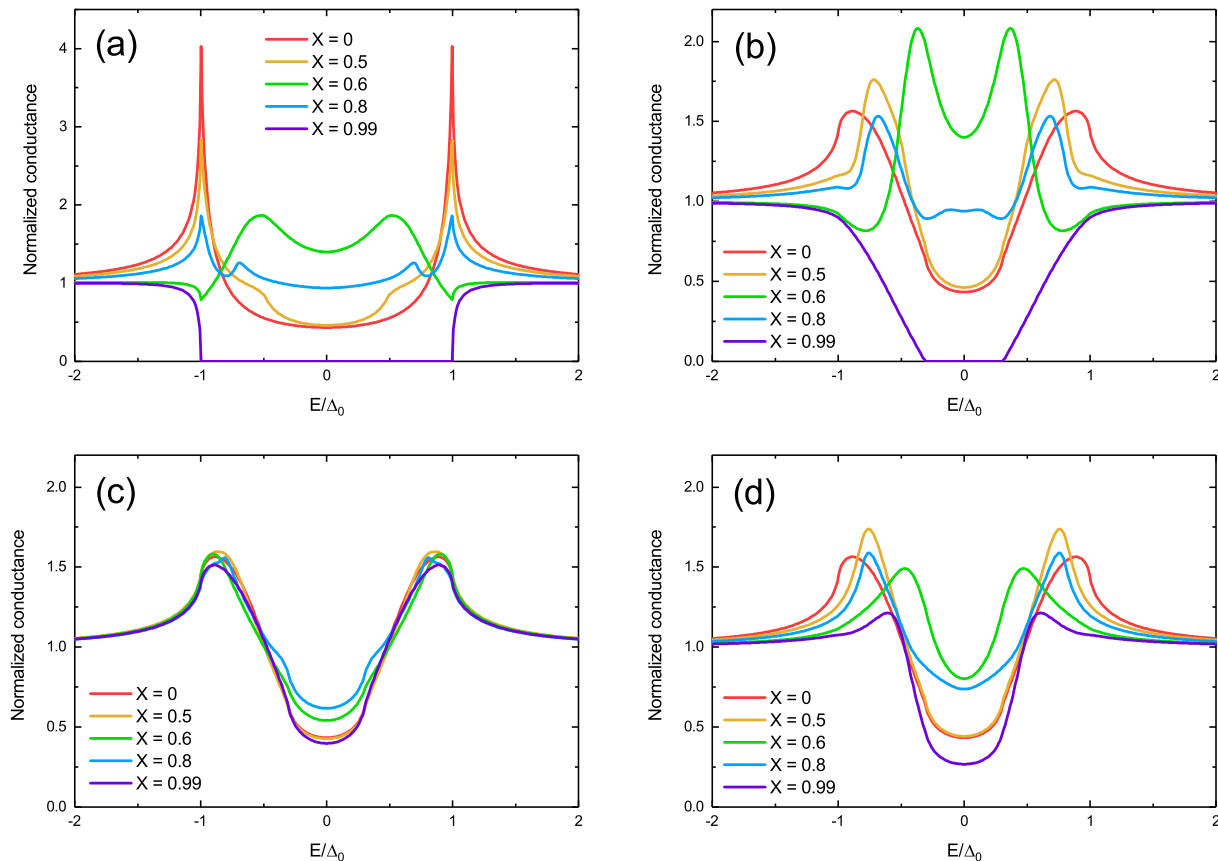


FIG. 3. Dimensionless tunneling conductance using pair potentials (a) SW, (b) CPW, $\theta_M = 0$, (c) HPW, $\theta_M = 0$ which is identical to CPW, $\theta_M = \pi/2$ and (d) HPW, $\theta_M = \pi/2$. Magnetization strengths varying from $X = 0$ (normal metal) to $X = 0.99$ (fully polarized). $Z_1 = 0.8$, $k_F L = 11$.

2(c), respectively. The blue and red lines represent the results for $\theta_M = 0$ and $\pi/2$, respectively.

The cases with and without N/F interface barrier are indicated by the solid and dashed lines, respectively. The results of the CPW, $\theta_M = 0$ case are similar to the SW case; there are two peaks around $E \approx 0.6\Delta_0$ and a dip at zero-energy. The position of the peaks is determined by the F thickness (L) and the magnitude of the magnetization ($X \equiv M/\mu$). In the CPW case, the Hamiltonian becomes equivalent to that for the SW case, except for the amplitude of the pair potential. Therefore, the corresponding results are qualitatively the same.

In the present case, the experimentally observed zero-bias conductance peak (ZBCP)^{22,23} does not appear. The Andreev bound states in CPW and HPW superconductors are located in the b - c and c - a planes. The junction under consideration is, however, along the c -axis, implying that these Andreev bound states cannot contribute to the differential conductance.⁷²

Comparing the red line in Fig. 2(b) to the blue line in Fig. 2(c), we find that the conductance spectra of CPW with $\theta_M = \pi/2$ and HPW with $\theta_M = 0$ are identical. In both cases, the d -vector is perpendicular to the magnetization ($\vec{d} \perp \mathbf{M}$), i.e., the total spin of the Cooper pairs

is parallel to the magnetization.

By analytically rotating the spin quantization axis, we reduce the matrix form of the pair potential matrix in the proper spin axis in which the z -direction is parallel to the magnetization. By doing this, we demonstrate that the pair potentials in the CPW, $\theta_M = \pi/2$ and HPW, $\theta_M = 0$ cases are qualitatively the same, except for the spin-dependent chirality. A full derivation is given in Appendix C; the matrix structures of the pair potential are summarized in table I. Hence, as far as there is no perturbation which mixes the spins or depends on the chirality (e.g., spin-active interface, spin-orbit coupling, or perturbation which breaks translational symmetry in x and/or y direction such as walls and impurities), it is impossible to distinguish between these two cases.

B. Amplitude of the magnetization

The effects of the amplitude of the magnetization are shown in Fig. 3, where the pair potential and the direction of the magnetization are set to (a) SW with $\theta_M = 0$, (b) CPW with $\theta_M = 0$, (c) CPW with $\theta_M = \pi/2$, and (d) HPW with $\theta_M = \pi/2$. We note that the result for the

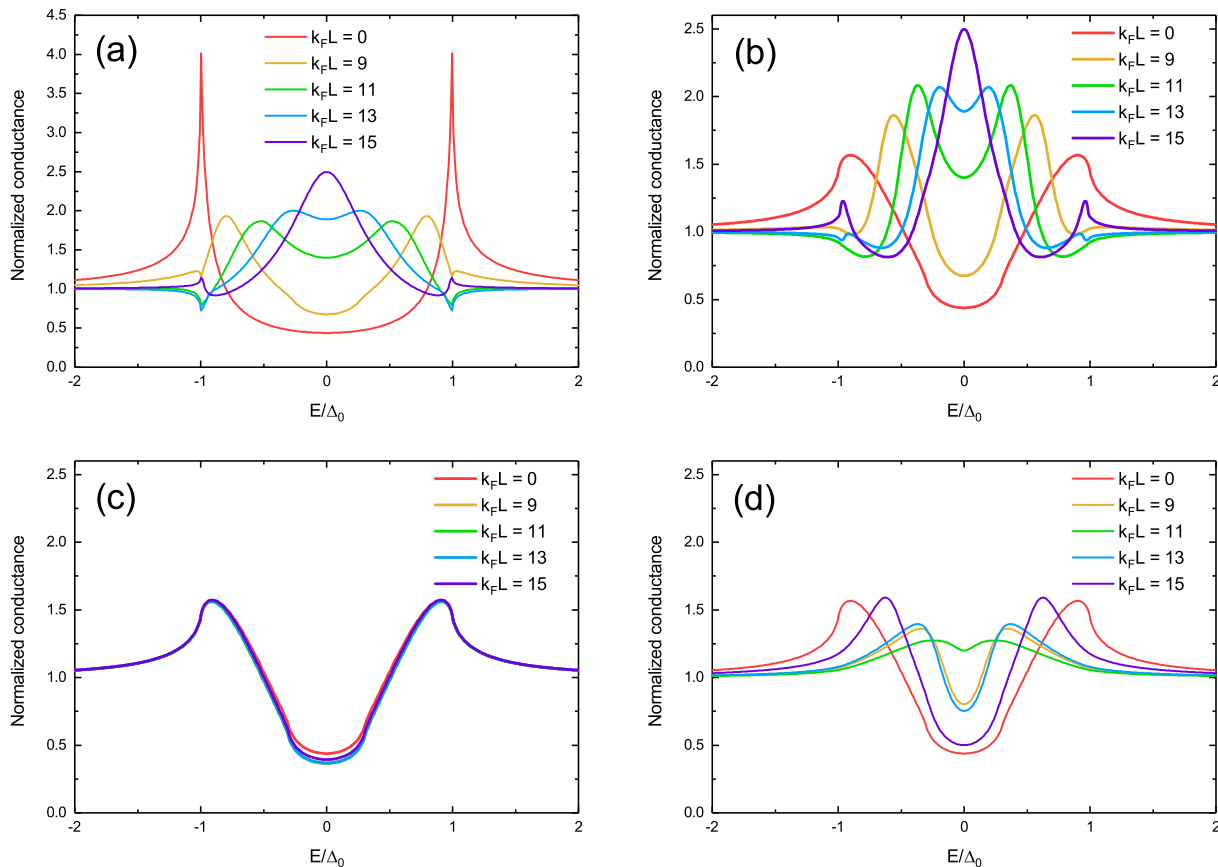


FIG. 4. The dimensionless tunneling conductance using pair potentials (a) SW, (b) CPW, $\theta_M = 0$, (c) HPW, $\theta_M = 0$ which is identical to CPW, $\theta_M = \pi/2$ and (d) HPW, $\theta_M = \pi/2$. Without ferromagnet ($k_F L = 0$) and for varying thicknesses $k_F L$ of the ferromagnet. $Z_1 = 0.8$, $X = 0.6$.

CPW with $\theta_M = \pi/2$ and that the HPW with $\theta_M = 0$ are identical to each other. The barrier strength and the thickness of the ferromagnet are set to $Z_1 = 0.8$ and $k_F L = 11$, respectively.

In the SW case in the absence of magnetization ($X = 0$), we obtain the BTK-like U-shaped spectrum⁶⁸ as shown in Fig. 3(a). Since the system is regarded as a N/N/S junction when $X = 0$, this result is well understood within the BTK theory. When the ferromagnet is fully spin polarised ($X \approx 1$), the conductance becomes zero in the energy range $|E| < \Delta_0$. Since there is no propagating channel in the S, a quasi particle with energy $|E| < \Delta_0$ must be either normally or Andreev reflected at the F/S interface. In spin-singlet superconductors, Andreev reflection is always accompanied by a spin flip (e.g., an up-spin particle is reflected as a down-spin hole). On the other hand, there is only one band in a fully-polarized ferromagnet, which implies that Andreev reflection is prohibited. As a result, the conductance in the energy range $|E| < \Delta_0$ is always zero. For moderate spin polarizations, the conductance spectra have complex structures that are sensitive to the amplitude of \mathbf{M} .

The conductance spectrum in the CPW, $\theta_M = 0$ case [Fig. 3(b)] is qualitatively the same as the SW spectrum,

because Cooper pairs consist of quasi particles with opposite spin. However, the CPW conductance changes more gradually as a function of magnetization because the amplitude of the pair potential changes depending on k_z . In the cases where $\mathbf{d} \perp \mathbf{M}$ [Fig. 3(c)], the conductance spectra do not depend on \mathbf{M} qualitatively because the total spin of the Cooper pairs aligns with the magnetization. This implies that the presence of the ferromagnet does not affect the superconductivity and therefore, the conductance spectra are insensitive to the magnetization. Contrary to Figs. 3(a) and 3(b), the conductance in the HPW, $\theta_M = \pi/2$ case [Fig. 3(d)] remains finite even if $X \approx 1$. In HPW superconductors, the d -vector lies in the xy -plain in spin space. Therefore, the \mathbf{k}_{\parallel} dependent part of the Andreev reflection is suppressed by the magnetization in the x -direction.

C. Thickness of the ferromagnet

In Fig. 4, the conductance spectra are plotted for several thicknesses of the ferromagnetic layer L . In the SW junction [Fig. 4(a)], the conductance shows the BTK-like U-shaped spectrum⁶⁸ as seen in Fig. 3(a) with $X = 0$.

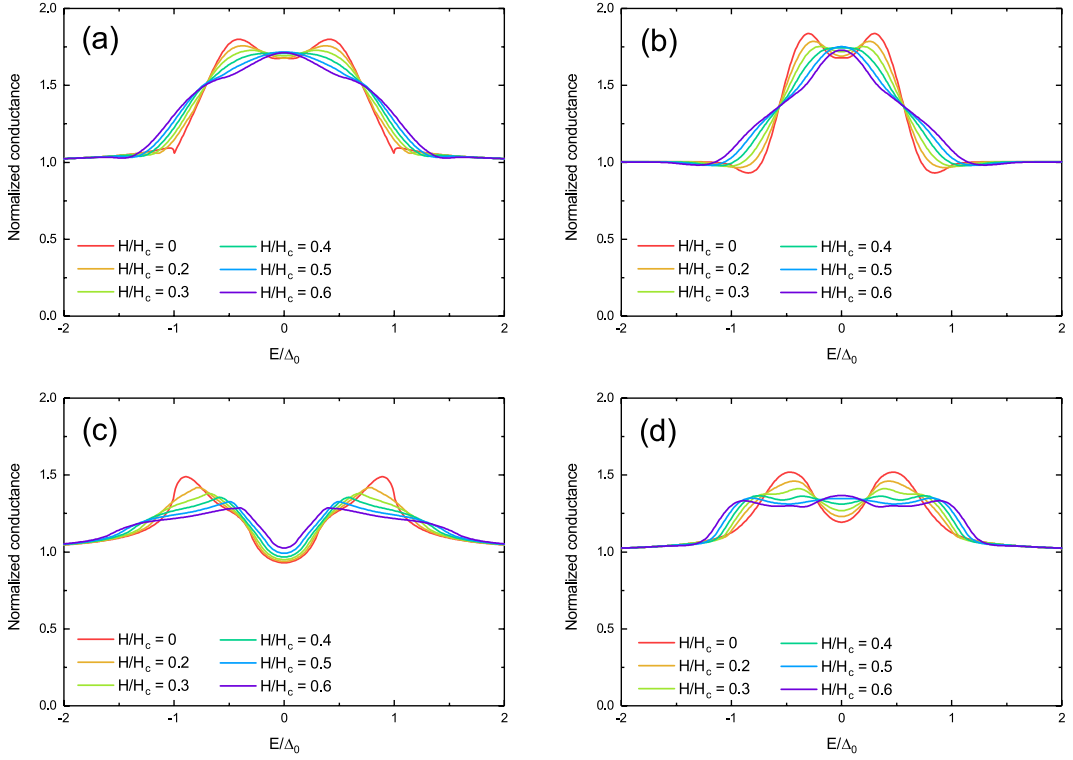


FIG. 5. Effects of an external magnetic field on the dimensionless tunneling conductance in the *absence* of the barrier potential. The pair potential is assumed to be (a) SW, (b) CPW, $\theta_M = 0$, (c) HPW, $\theta_M = 0$, and (d) HPW, $\theta_M = \pi/2$. The results for the CPW with $\theta_M = \pi/2$ are identical to the results in the panel (c). The parameters are set to $Z_1 = 0$, $X = 0.6$, and $k_F L = 11$.

The distance between the two peaks decreases with increasing thickness. Simultaneously, the structures at $E = \Delta_0$ change from peaks to dips. When $k_F L = 15$, the two peaks merge into a ZBCP. We note that this peak is different from the well-known ZBCP in d -wave superconductors, which stems from the interference between incident and reflected quasi particles at the interface. On the other hand, the peak at the zero-energy in Fig. 3(a) is formed by an accidental constructive Fabry-Perot interference in the ferromagnet.⁷³ Hence, this peak is not robustly resistant to impurities and is therefore not related to the topology in the superconductor.

Similar behaviour is seen in the spectrum of the CPW with $\theta_M = 0$ case [Fig. 4(b)]. In HPW superconductors [Fig. 4(d)], the distance between the two peaks first reduces for $0 \leq k_F L \leq 11$, whereas it increases for $11 \leq k_F L \leq 15$. However, the constructive interference as seen in CPW superconductors never occurs at the zero energy. This is a significant difference between CPW and HPW superconductors.

When the d -vector is perpendicular to the magnetization (i.e., $\vec{d} \perp \mathbf{M}$), the results are insensitive to the ferromagnet thickness, as shown in Fig. 4(c). This can also be interpreted in terms of the relation between the direction of \mathbf{M} and the total spin of Cooper pairs in the superconductor.

D. External magnetic field

The magnetic field dependence of the conductance in the absence (presence) of a barrier at the N/F interface is shown in Fig. 5 (Fig. 6), where the other parameters are set to the same values used in Fig. 3. The pair potential is assumed to be (a) SW, (b) CPW with $\theta_M = 0$, (c) CPW with $\theta_M = \pi/2$, and (d) HPW with $\theta_M = \pi/2$, where the results for the HPW with $\theta_M = 0$ are identical to the results in panel (c). We show only the results for an external field $H \leq 0.6H_c$, since the effects of the nucleation of vortices are not taken into account.

In general, the Doppler shift causes peaks to split into two smaller peaks, which shift with k_{\parallel} , as follows from Eq. (A7). Since pairing symmetries have different k_{\parallel} -dependencies, the evolution of the peak shape is different in each case. Both SW and CPW with $\theta_M = 0$ [Figs. 5(a) and 5(b)] show a three dip structure that gradually transitions into a broad ZBCP. For the CPW with $\theta_M = \pi/2$ and HPW with $\theta_M = 0$ cases [Fig. 5(c)], the coherence peaks are smeared out by the magnetic field, although the central dip remains. In the HPW with $\theta_M = \pi/2$ case [Fig. 5(d)], the two peaks are split into four smaller peaks [$H/H_c = 0.4$ in Fig. 5(d)]. The outer peaks shift to away from zero energy, while the inner ones merge and form a small ZBCP.

Including a barrier in the SW, both CPW and HPW,

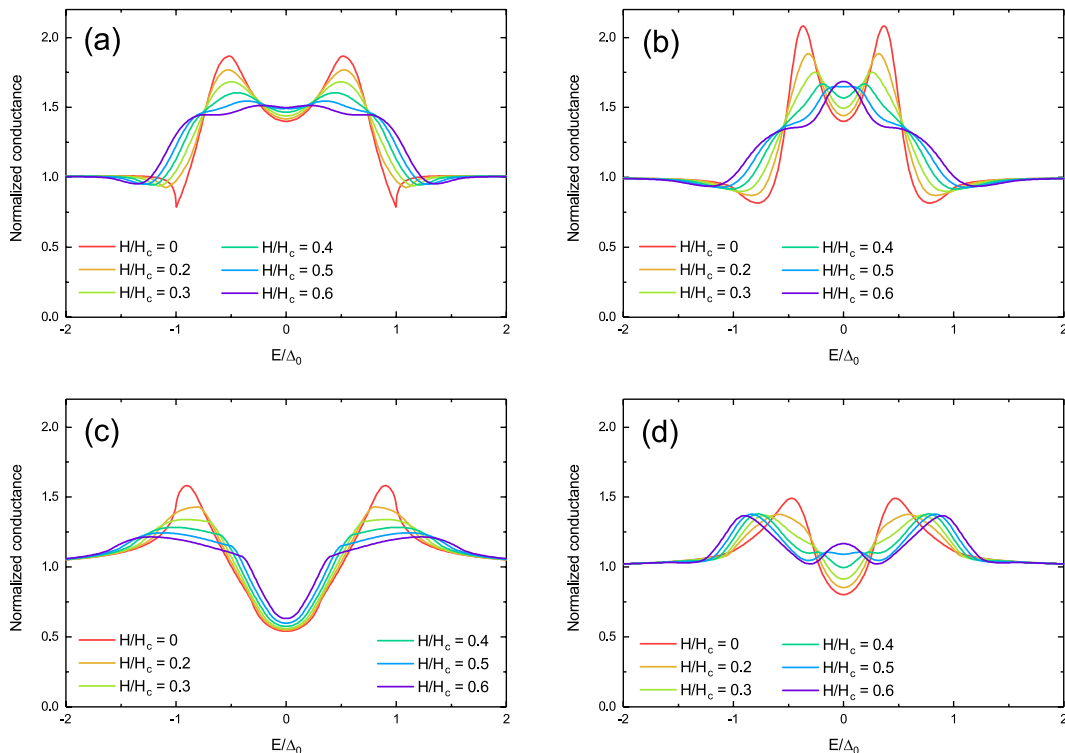


FIG. 6. Effects of an external magnetic field on the dimensionless tunneling conductance in the *presence* of the barrier potential $Z_1 = 0.8$ in the same manner as in Fig. 5.

$\theta_M = 0$ cases [Figs. 6(a)-6(c)] does not change the behaviour qualitatively, but the overall structure is more pronounced. In the HPW, $\theta_M = \pi/2$ case [Fig. 6(d)], however, the spectrum changes from a plateau to a three-peak structure. The CPW, $\theta_M = 0$ and HPW, $\theta_M = \pi/2$ cases can be distinguished by looking at the relative peak height of the ZBCP.

IV. SUMMARY

We have investigated the conductance of a N/F/S junction with various pair potentials as a function of ferromagnetic properties (thickness, magnetization strength and direction). The SW and CPW, $\theta_M = 0$ cases are similar, although the latter shows a more rounded conductance due to the angle dependence of the pair potential. We found that the cases where the d -vector is perpendicular to the magnetization direction (CPW, $\theta_M = \pi/2$ and HPW, $\theta_M = 0$) are identical. In these cases, the opposite spins parts of the Hamiltonian are decoupled and therefore, they are insensitive to the ferromagnet thickness and magnetization strength. The cases where the d -vector is parallel to the magnetization direction are very different due to a more complex structure. The main difference is that CPW, $\theta_M = 0$ converges to a zero energy peak for $k_FL = 15$, while HPW, $\theta_M = \pi/2$ shows a dip. In the presence of an external magnetic field, the evolution of the conductance spectra depends on the pairing symme-

try. In particular, the CPW, $\theta_M = 0$ case gives an accidental ZBCP. The central dip in the CPW, $\theta_M = \pi/2$ and HPW, $\theta_M = 0$ cases remains. In the HPW, $\theta_M = \pi/2$ case, the structure depends on the barrier strength; a plateau or three peaks.

For future research, it would be interesting to take higher applied magnetic fields into account by including Abrikosov vortices. To obtain a more accurate representation of the Sr_2RuO_4 , tunneling spectroscopy can be simulated using a multiband model.^{74,75}

ACKNOWLEDGMENTS

This work was supported by JSPS Core-to-Core program ‘‘Oxide Superspin’’ international network, a Grant-in-Aid for Scientific Research on Innovative Areas Topological Material Science JPSJ KAKENHI (Grants No. JP15H05851, No. 15H05852, No. JP15H05853, and No. JP15K21717), and a Grant-in-Aid for Scientific Research B (Grant No. JP15H03686 and JP18H01176). It was also supported by JSPS-RFBR Bilateral Joint Research Projects and Seminars Grant No. 17-52-50080, the Ministry of Education and Science of the Russian Federation Grant No. 14.Y26.31.0007 and by joint Russian-Greek projects RFMEFI61717X0001 and T4ΔPΩ-00031.

Appendix A: Doppler shift

In the presence of a magnetic field $\mathbf{H} = \nabla \times \mathbf{A}$ the canonical momentum operator \mathbf{p} is replaced by the kinetic momentum operator $\boldsymbol{\pi} = \mathbf{p} - e\mathbf{A}(\vec{r})/c$. As a result, the quasi particle kinetic energy ξ_k becomes

$$\xi_k = \frac{1}{2m} \boldsymbol{\pi} \cdot \boldsymbol{\pi} - \mu = -\frac{\hbar^2}{2m} \left(\nabla - i \frac{|e|}{\hbar c} \mathbf{A} \right)^2 - \mu. \quad (\text{A1})$$

where μ is the chemical potential. In the weak-coupling limit ($\Delta_0 \ll \mu$), this can be approximated by

$$\xi_k \approx -\frac{\hbar^2 \nabla^2}{2m} - i \frac{\hbar |e|}{mc} \nabla \cdot \mathbf{A} - \mu. \quad (\text{A2})$$

In our case, an external magnetic field \mathbf{H} is applied in the x -direction. Hence, the magnetic field and vector potential for $z \geq 0$ are approximately⁷⁶

$$\mathbf{H}(z) = H e^{-z/\lambda_L} \mathbf{e}_x, \quad (\text{A3})$$

$$\mathbf{A}(z) = -H \lambda_L e^{-z/\lambda_L} \mathbf{e}_y, \quad (\text{A4})$$

where λ_L is the London penetration depth. The spatial dependence of \mathbf{A} is characterized by λ_L , whereas the Cooper pair wave function is characterized by the coherence length ξ_0 . In the type-II limit ($\lambda_L/\xi_0 \gg 1$), the spatial dependence of \mathbf{A} does not change the differential conductance. Therefore we introduce the constant vector potential⁷⁷

$$\mathbf{A}(z) \approx -H \lambda_L \mathbf{e}_y. \quad (\text{A5})$$

This linear response is only valid in the absence of vortices, i.e. for small magnetic fields ($H \leq 0.6H_c$). Assuming plane waves in the x - and y -direction, the wave function can be written as $\psi(x, y, z) = \psi(z) e^{ik_x x} e^{ik_y y}$, such that Eq. (A2) becomes

$$\xi_k = -\frac{\hbar^2}{2m} \frac{\partial^2}{\partial z^2} + \frac{\hbar^2 k_{\parallel}^2}{2m} - \frac{\hbar |e|}{mc} H \lambda_L k_y - \mu, \quad (\text{A6})$$

where $k_{\parallel}^2 = k_x^2 + k_y^2$. Defining $\mu' \equiv \mu - \hbar^2 k_{\parallel}^2 / 2m$ and substituting $H_c = \phi_0 / \pi \xi_0 \lambda_L$, $\phi_0 = \pi \hbar c / |e|$, $\xi_0 = \hbar v_F / \Delta_0$, $k_y = k_{\parallel} \sin \varphi$ and $v_F = \hbar k_F / m$, Eq. (A6) can be written as

$$\xi_k = -\frac{\hbar^2}{2m} \frac{\partial^2}{\partial z^2} - \mu' - \Delta_0 \frac{H}{H_c} \frac{k_{\parallel}}{k_F} \sin \varphi, \quad (\text{A7})$$

where H_c is the thermodynamical critical field.

Appendix B: Numerical method

Substituting wave functions Eqs. (17) and (20) into boundary condition Eq. (31) gives

$$\vec{i} + \vec{r} = \check{A} \left(\vec{f}_p + \vec{f}_n \right). \quad (\text{B1})$$

We do the same with boundary condition Eq. (32) and divide by ik_0 for normalization, where we define k_0 as the momentum in the normal metal, i.e. $k_0 = \sqrt{2m_N \mu} / \hbar$. The second boundary condition becomes

$$\left(\frac{k_N}{k_0} \check{\tau}_0 - 2i \check{Z}_1 \right) \vec{i} - \left(\frac{k_N}{k_0} \check{\tau}_z + 2i \check{Z}_1 \right) \vec{r} = \check{A} \check{Q} \left(\vec{f}_p - \vec{f}_n \right) \quad (\text{B2})$$

where $\check{Q} = \text{diag}[k_F^+, k_F^-, k_F^+, k_F^-] / k_0$ and \check{Z}_1 is the dimensionless barrier strength of the first interface, given by

$$\check{Z}_1 = \frac{m(z) \check{F}_1}{\hbar^2 k_0}. \quad (\text{B3})$$

We substitute wave functions Eqs. (20) and (24) into the third boundary condition, Eq. (33), to obtain

$$\check{A} \check{K}_F^{L+} \vec{f}_p + \check{A} \check{K}_F^{L-} \vec{f}_n = \check{U} \check{K}_S^L \vec{t}, \quad (\text{B4})$$

where we used $\check{K}_F^{L\pm} = \check{K}_F^{\pm}|_{z=L}$ and $\check{K}_S^{L\pm} = \check{K}_S^{\pm}|_{z=L}$ for abbreviation. Similarly, from Eq. (34), we get

$$\begin{aligned} \check{A} \check{Q} \left(\check{K}_F^{L+} \vec{f}_p - \check{K}_F^{L-} \vec{f}_n \right) - 2i \check{Z}_{\text{SO}} \check{A} \left(\check{K}_F^{L+} \vec{f}_p + \check{K}_F^{L-} \vec{f}_n \right) \\ = \frac{k_S}{k_0} \check{U} \check{\tau}_z \check{K}_S^L \vec{t}, \end{aligned} \quad (\text{B5})$$

where \check{Z}_{SO} is the dimensionless spin-orbit coupling strength at the second interface, defined as

$$\check{Z}_{\text{SO}} = \frac{m(z) \check{F}_{\text{SO}}}{\hbar^2 k_0}. \quad (\text{B6})$$

Eqs. (B1), (B2), (B4), (B5) form a system of 16 equations with 16 unknowns. Substituting Eqs. (B4) and (B5) into one another, we can write $\check{M}_1 \vec{f}_p = \check{M}_2 \vec{f}_n$, with

$$\begin{aligned} \check{M}_1 &= \check{A} \check{Q} \check{K}_F^{L+} - 2i \check{Z}_{\text{SO}} \check{A} \check{K}_F^{L+} - \frac{k_S}{k_0} \check{U} \check{\tau}_z \check{U}^{-1} \check{A} \check{K}_F^{L+}, \\ \check{M}_2 &= \check{A} \check{Q} \check{K}_F^{L-} + 2i \check{Z}_{\text{SO}} \check{A} \check{K}_F^{L-} + \frac{k_S}{k_0} \check{U} \check{\tau}_z \check{U}^{-1} \check{A} \check{K}_F^{L-}. \end{aligned}$$

Combining this with Eq. (B2), we can express \vec{f}_p and \vec{f}_n in terms of \vec{i} and \vec{r} as

$$\vec{f}_n = \check{M}_3^{-1} (\vec{i} + \vec{r}) \quad (\text{B7})$$

$$\vec{f}_p = \check{M}_1^{-1} \check{M}_2 \check{M}_3^{-1} (\vec{i} + \vec{r}), \quad (\text{B8})$$

where $\check{M}_3 = \check{A} (\check{M}_1^{-1} \check{M}_2 + \check{\tau}_0)$. Substituting Eqs. (B7) and (B8) into Eq. (B1), we find that

$$\vec{r} = \check{M}_4^{-1} \check{M}_5 \vec{i} \quad (\text{B9})$$

with

$$\check{M}_4 = \frac{k_N}{k_0} \check{\tau}_z + 2i \check{Z}_1 - \check{A} \check{Q} (\check{M}_1^{-1} \check{M}_2 - \check{\sigma}_0) \check{M}_3^{-1},$$

$$\check{M}_5 = \frac{k_N}{k_0} \check{\tau}_0 - 2i \check{Z}_1 + \check{A} \check{Q} (\check{M}_1^{-1} \check{M}_2 - \check{\sigma}_0) \check{M}_3^{-1}.$$

Using the \vec{r} coefficients, the conductance can be determined by Eq. (36).

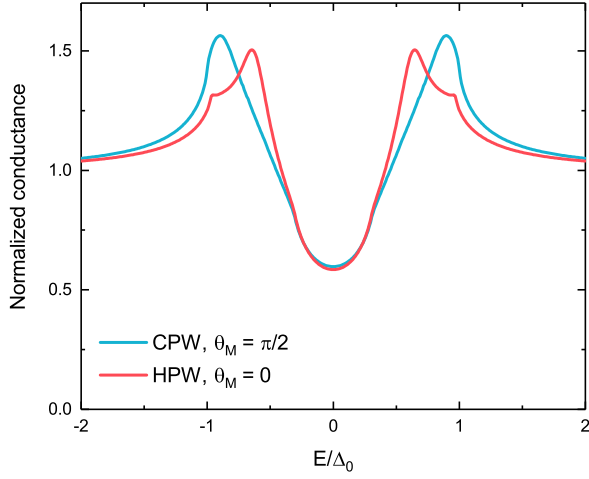


FIG. 7. The dimensionless tunneling conductance for CPW, $\theta_M = \pi/2$ and HPW, $\theta_M = 0$, including spin-orbit coupling $Z_{SO} = 1$, $Z_1 = 0.8$, $X = 0.6$, $k_F L = 11$.

Appendix C: Rotation of spin quantisation axis

To discuss the spin of Cooper pairs, it is convenient to rotate the spin quantization axis such that the new z -axis is parallel to the magnetization \mathbf{M} . In our case, \mathbf{M} is in the xz -plane in spin space. Therefore, the rotation should be around the y -axis in spin space, which is carried out by the unitary operator

$$\hat{U}(\theta_M) = \exp[i(\theta_M/2)\hat{\sigma}_y] \quad (\text{C1})$$

$$= \hat{\sigma}_0 \cos(\theta_M/2) + i\hat{\sigma}_y \sin(\theta_M/2), \quad (\text{C2})$$

with which we can rotate spin space by an angle θ_M . The unitary matrix in Eq. (C2) satisfies $\hat{U}^* = \hat{U}$ and therefore, the unitary matrix in Nambu space is given by $\tilde{U} = \text{diag}[\hat{U}, \hat{U}^*] = \text{diag}[\hat{U}, \hat{U}]$. The BdG equation changes accordingly and becomes

$$\tilde{H}\tilde{\Psi} = E\tilde{\Psi} \quad \rightarrow \quad \tilde{H}'\tilde{\Psi} = E\tilde{\Psi}, \quad (\text{C3})$$

with

$$\tilde{\Psi} = \tilde{U}\Psi, \quad \tilde{H}' = \tilde{U}\tilde{H}\tilde{U}^\dagger, \quad (\text{C4})$$

$$\Psi = \begin{bmatrix} \psi_\uparrow & \psi_\downarrow & \psi_\uparrow^\dagger & \psi_\downarrow^\dagger \end{bmatrix}^T. \quad (\text{C5})$$

Only the magnetization term depends on spin in the single-particle Hamiltonian $\hat{h}(z)$. In the new spin basis, the magnetization term for particles and holes is given by, respectively,

$$\hat{U}(\mathbf{M} \cdot \hat{\boldsymbol{\sigma}})\hat{U}^\dagger = M\hat{\sigma}_z, \quad (\text{C6})$$

$$\hat{U}(-\mathbf{M} \cdot \hat{\boldsymbol{\sigma}}^*)\hat{U}^\dagger = -M\hat{\sigma}_z. \quad (\text{C7})$$

The pair potential in the new spin space is

$$\begin{bmatrix} \hat{\Delta}_{\mathbf{k}_\parallel} \\ -\hat{\Delta}_{-\mathbf{k}_\parallel}^* \end{bmatrix} \rightarrow \begin{bmatrix} \hat{U}\hat{\Delta}_{\mathbf{k}_\parallel}\hat{U}^\dagger \\ -[\hat{U}\hat{\Delta}_{-\mathbf{k}_\parallel}\hat{U}^\dagger]^* \end{bmatrix}, \quad (\text{C8})$$

where we used the relation $\hat{U}^* = \hat{U}$. The superconducting pair potential $\hat{\Delta}_{\mathbf{k}_\parallel}$ is transformed to

$$\begin{aligned} & \hat{U}\hat{\Delta}_{\mathbf{k}_\parallel}\hat{U}^\dagger \\ &= \begin{cases} \Delta_0 i\hat{\sigma}_y & \text{for SW,} \\ \Delta_0(\bar{k}_x + i\chi\bar{k}_y)[\cos\theta\hat{\sigma}_x + \sin\theta\hat{\sigma}_z] & \text{for CPW,} \\ \Delta_0(\bar{k}_x\hat{\sigma}_0 + i\bar{k}_y[\cos\theta\hat{\sigma}_z - \sin\theta\hat{\sigma}_x]) & \text{for HPW.} \end{cases} \end{aligned} \quad (\text{C9})$$

If we substitute $\theta_M = 0, \pi/2$, these expressions reduce to the pair potentials in table I in the main text.

We focus on CPW, $\theta_M = \pi/2$ and HPW, $\theta_M = 0$. In both cases, the magnetization \mathbf{M} is perpendicular to the d -vector. In other words, \mathbf{M} and the total spin of Cooper pairs are collinear. Therefore, the magnetization does not destroy the Cooper pairs. The 4×4 Hamiltonian matrix can be reduced to two 2×2 matrices:

$$\begin{aligned} \mathcal{H} &= \frac{1}{2} \sum_{\mathbf{k}_\parallel} \int \tilde{\Psi}^\dagger(z) \tilde{H}_B(z) \tilde{\Psi}(z) dz, \\ &= \frac{1}{2} \sum_{\mathbf{k}_\parallel} \int \sum_{\alpha=\pm 1} \tilde{\Psi}_\alpha^\dagger \begin{bmatrix} \xi + \alpha M & \Delta_{\alpha, \mathbf{k}_\parallel} \\ -\Delta_{\alpha, -\mathbf{k}_\parallel}^* & -(\xi + \alpha M) \end{bmatrix} \tilde{\Psi}_\alpha dz. \end{aligned} \quad (\text{C10})$$

We have introduced a new basis which depends on the spin sector α : $\tilde{\Psi}_\alpha(z) = [\tilde{\psi}_\alpha(z) \tilde{\psi}_\alpha^\dagger(z)]$. Eq. (C10) implies that the system can be decomposed into the spin-up ($\alpha = 1$) and spin-down ($\alpha = -1$) subsystems, where we have redefined the up and down spins for the new spin quantization axis. The α -dependent pair potential is given by

$$\Delta_{\alpha, \mathbf{k}_\parallel} = \begin{cases} \alpha\Delta_0 e^{i\phi} & \text{for CPW, } \theta_M = \pi/2, \\ \Delta_0 e^{i\alpha\phi} & \text{for HPW, } \theta_M = 0, \end{cases} \quad (\text{C11})$$

where we fix $\chi = 1$. In the CPW, $\theta_M = \pi/2$ case, the chiralities for up- and down-spin sectors are the same, while the signs of the α -dependent pair potential are opposite. In the HPW, $\theta_M = 0$ case, the chiralities are opposite, while the signs of the α -dependent pair potential are equal. Therefore, as far as there is no perturbation which mixes the spins or depends on the chirality (*e.g.*, spin-active interface, spin-orbit coupling and perturbations which breaks translational symmetry in the x and/or y direction such as walls and impurities), it is impossible to distinguish these two cases.

This is demonstrated in Fig. 7, where we introduced spin-orbit coupling at the F/S interface by setting $Z_{SO} =$

1. In the absence spin-orbit coupling, these two graphs overlapped as seen in Figs. 3(c), 4(c), 5(c), and 6(c).

However, in Fig. 7, we can see that they are indeed slightly different.

-
- ¹ Y. Maeno, H. Hashimoto, K. Yoshida, S. Nishizaki, T. Fujita, J. G. Bednorz, and F. Lichtenberg, *Nature* **372**, 532 (1994).
- ² K. Ishida, H. Mukuda, Y. Kitaoka, K. Asayama, Z. Q. Mao, Y. Mori, and Y. Maeno, *Nature* **396**, 658 (1998).
- ³ H. Tou, Y. Kitaoka, K. Ishida, K. Asayama, N. Kimura, Y. Onuki, E. Yamamoto, Y. Haga, and K. Maezawa, *Physical Review Letters* **80**, 3129 (1998).
- ⁴ H. Murakawa, K. Ishida, K. Kitagawa, Z. Q. Mao, and Y. Maeno, *Phys. Rev. Lett.* **93**, 167004 (2004).
- ⁵ A. P. Mackenzie and Y. Maeno, *Rev. Mod. Phys.* **75**, 657 (2003).
- ⁶ Y. Maeno, S. Kittaka, T. Nomura, S. Yonezawa, and K. Ishida, *Journal of the Physical Society of Japan* **81**, 011009 (2012).
- ⁷ T. M. Rice and M. Sigrist, *Journal of Physics: Condensed Matter* **7**, L643 (1995).
- ⁸ K. Miyake and O. Narikiyo, *Phys. Rev. Lett.* **83**, 1423 (1999).
- ⁹ T. Kuwabara and M. Ogata, *Phys. Rev. Lett.* **85**, 4586 (2000).
- ¹⁰ T. Nomura and K. Yamada, *Journal of the Physical Society of Japan* **69**, 3678 (2000).
- ¹¹ T. Nomura and K. Yamada, *Journal of the Physical Society of Japan* **71**, 404 (2002).
- ¹² T. Nomura and K. Yamada, *Journal of the Physical Society of Japan* **71**, 1993 (2002).
- ¹³ R. Arita, S. Onari, K. Kuroki, and H. Aoki, *Phys. Rev. Lett.* **92**, 247006 (2004).
- ¹⁴ T. Nomura and K. Yamada, *Journal of the Physical Society of Japan* **74**, 1818 (2005).
- ¹⁵ T. Nomura, D. S. Hirashima, and K. Yamada, *Journal of the Physical Society of Japan* **77**, 024701 (2008).
- ¹⁶ Y. Yanase and M. Ogata, *Journal of the Physical Society of Japan* **72**, 673 (2003).
- ¹⁷ S. Raghu, A. Kapitulnik, and S. A. Kivelson, *Phys. Rev. Lett.* **105**, 136401 (2010).
- ¹⁸ M. Sato and M. Kohmoto, *Journal of the Physical Society of Japan* **69**, 3505.
- ¹⁹ K. Kuroki, M. Ogata, R. Arita, and H. Aoki, *Phys. Rev. B* **63**, 060506 (2001).
- ²⁰ T. Takimoto, *Phys. Rev. B* **62**, R14641 (2000).
- ²¹ M. Tsuchiizu, Y. Yamakawa, S. Onari, Y. Ohno, and H. Kontani, *Phys. Rev. B* **91**, 155103 (2015).
- ²² F. Laube, G. Goll, H. v. Löhneysen, M. Fogelström, and F. Lichtenberg, *Phys. Rev. Lett.* **84**, 1595 (2000).
- ²³ Z. Q. Mao, K. D. Nelson, R. Jin, Y. Liu, and Y. Maeno, *Phys. Rev. Lett.* **87**, 037003 (2001).
- ²⁴ Y. Tanaka and S. Kashiwaya, *Phys. Rev. Lett.* **74**, 3451 (1995).
- ²⁵ S. Kashiwaya and Y. Tanaka, *Rep. Prog. Phys.* **63**, 1641 (2000).
- ²⁶ M. Yamashiro, Y. Tanaka, and S. Kashiwaya, *Phys. Rev. B* **56**, 7847 (1997).
- ²⁷ S. Kashiwaya, H. Kashiwaya, H. Kambara, T. Furuta, H. Yaguchi, Y. Tanaka, and Y. Maeno, *Phys. Rev. Lett.* **107**, 077003 (2011).
- ²⁸ M. Yamashiro, Y. Tanaka, Y. Tanuma, and S. Kashiwaya, *J. Phys. Soc. Jpn.* **67**, 3224 (1998).
- ²⁹ C. Honerkamp and M. Sigrist, *Journal of Low Temperature Physics* **111**, 895 (1998).
- ³⁰ S. Kashiwaya, Y. Tanaka, M. Koyanagi, H. Takashima, and K. Kajimura, *Phys. Rev. B* **51**, 1350 (1995).
- ³¹ S. Kashiwaya, Y. Tanaka, N. Terada, M. Koyanagi, S. Ueno, L. Alff, H. Takashima, Y. Tanuma, and K. Kajimura, *J. Phys. Chem. Solid* **59**, 2034 (1998).
- ³² M. Covington, M. Aprili, E. Paraoanu, L. H. Greene, F. Xu, J. Zhu, and C. A. Mirkin, *Phys. Rev. Lett.* **79**, 277 (1997).
- ³³ L. Alff, H. Takashima, S. Kashiwaya, N. Terada, H. Ihara, Y. Tanaka, M. Koyanagi, and K. Kajimura, *Phys. Rev. B* **55**, R14757 (1997).
- ³⁴ J. Y. T. Wei, N.-C. Yeh, D. F. Garrigus, and M. Strask, *Phys. Rev. Lett.* **81**, 2542 (1998).
- ³⁵ I. Iguchi, W. Wang, M. Yamazaki, Y. Tanaka, and S. Kashiwaya, *Phys. Rev. B* **62**, R6131 (2000).
- ³⁶ C. R. Hu, *Phys. Rev. Lett.* **72**, 1526 (1994).
- ³⁷ M. Sato, Y. Tanaka, K. Yada, and T. Yokoyama, *Phys. Rev. B* **83**, 224511 (2011).
- ³⁸ Y. Tanaka and S. Kashiwaya, *Phys. Rev. B* **70**, 012507 (2004).
- ³⁹ Y. Tanaka, S. Kashiwaya, and T. Yokoyama, *Phys. Rev. B* **71**, 094513 (2005).
- ⁴⁰ Y. Asano, Y. Tanaka, and S. Kashiwaya, *Phys. Rev. Lett.* **96**, 097007 (2006).
- ⁴¹ Y. Tanaka, Y. Asano, A. A. Golubov, and S. Kashiwaya, *Phys. Rev. B* **72**, 140503 (2005).
- ⁴² Y. Asano, A. A. Golubov, Y. V. Fominov, and Y. Tanaka, *Phys. Rev. Lett.* **107**, 087001 (2011).
- ⁴³ X.-L. Qi and S.-C. Zhang, *Rev. Mod. Phys.* **83**, 1057 (2011).
- ⁴⁴ G. M. Luke, Y. Fudamoto, K. M. Kojima, M. I. Larkin, J. Merrin, B. Nachumi, Y. J. Uemura, Y. Maeno, Z. Q. Mao, Y. Mori, H. Nakamura, and M. Sigrist, *Nature* **394**, 558.
- ⁴⁵ J. Xia, Y. Maeno, P. T. Beyersdorf, M. M. Fejer, and A. Kapitulnik, *Phys. Rev. Lett.* **97**, 167002 (2006).
- ⁴⁶ M. Matsumoto and M. Sigrist, *Journal of the Physical Society of Japan* **68**, 3120 (1999).
- ⁴⁷ J. Xia, Y. Maeno, P. T. Beyersdorf, M. M. Fejer, and A. Kapitulnik, *Phys. Rev. Lett.* **97**, 167002 (2006).
- ⁴⁸ J. R. Kirtley, C. Kallin, C. W. Hicks, E.-A. Kim, Y. Liu, K. A. Moler, Y. Maeno, and K. D. Nelson, *Phys. Rev. B* **76**, 014526 (2007).
- ⁴⁹ C. W. Hicks, J. R. Kirtley, T. M. Lippman, N. C. Koshnick, M. E. Huber, Y. Maeno, W. M. Yuhasz, M. B. Maple, and K. A. Moler, *Phys. Rev. B* **81**, 214501 (2010).
- ⁵⁰ W. Huang, E. Taylor, and C. Kallin, *Phys. Rev. B* **90**, 224519 (2014).
- ⁵¹ S. Lederer, W. Huang, E. Taylor, S. Raghu, and C. Kallin, *Phys. Rev. B* **90**, 134521 (2014).
- ⁵² P. E. C. Ashby and C. Kallin, *Phys. Rev. B* **79**, 224509 (2009).
- ⁵³ W. Huang, S. Lederer, E. Taylor, and C. Kallin, *Phys.*

- Rev. B **91**, 094507 (2015).
- ⁵⁴ A. Bouhon and M. Sigrist, Phys. Rev. B **90**, 220511 (2014).
- ⁵⁵ Y. Tada, N. Kawakami, and S. Fujimoto, New Journal of Physics **11**, 055070 (2009).
- ⁵⁶ S.-I. Suzuki and Y. Asano, Phys. Rev. B **94**, 155302 (2016).
- ⁵⁷ T. Hirai, N. Yoshida, Y. Tanaka, J. ichiro Inoue, and S. Kashiwaya, Journal of the Physical Society of Japan **70**, 1885 (2001).
- ⁵⁸ T. Hirai, Y. Tanaka, N. Yoshida, Y. Asano, J. Inoue, and S. Kashiwaya, Phys. Rev. B **67**, 174501 (2003).
- ⁵⁹ N. Yoshida, Y. Tanaka, J. Inoue, and S. Kashiwaya, Journal of the Physical Society of Japan **68**, 1071 (1999).
- ⁶⁰ H. Li and X. Yang, Solid State Communications **152**, 1655 (2012).
- ⁶¹ Q. Cheng and B. Jin, Physica B **426**, 40 (2013).
- ⁶² M. S. Anwar, S. R. Lee, R. Ishiguro, Y. Sugimoto, Y. Tano, S. J. Kang, Y. J. Shin, S. Yonezawa, D. Manske, H. Takayanagi, T. W. Noh, and Y. Maeno, Nature Commun. **7**, 13220 (2016).
- ⁶³ P. Gentile, M. Cuoco, A. Romano, C. Noce, D. Manske, and P. M. R. Brydon, Phys. Rev. Lett. **111**, 097003 (2013).
- ⁶⁴ D. Terrade, P. Gentile, M. Cuoco, and D. Manske, Phys. Rev. B **88**, 054516 (2013).
- ⁶⁵ P. M. R. Brydon and D. Manske, Phys. Rev. Lett. **103**, 147001 (2009).
- ⁶⁶ P. M. R. Brydon, Phys. Rev. B **80**, 224520 (2009).
- ⁶⁷ S. Wu and K. V. Samokhin, Phys. Rev. B **81**, 214506 (2010).
- ⁶⁸ G. E. Blonder, M. Tinkham, and T. M. Klapwijk, Phys. Rev. B **25**, 4515 (1982).
- ⁶⁹ We note that Eq. (35) is still valid in the presence of spin-rotation. SOC only influences the transport coefficients and does not affect the validity of Eq. (35).
- ⁷⁰ Y. J. Chang, C. H. Kim, S.-H. Phark, Y. S. Kim, J. Yu, and T. W. Noh, Phys. Rev. Lett. **103**, 057201 (2009).
- ⁷¹ C.-T. Wu, O. T. Valls, and K. Halterman, Phys. Rev. B **90**, 054523 (2014).
- ⁷² The condition under which the ABSs emerge is given by $\Delta(k_z)\Delta(-k_z) < 0$.⁷⁸ All pair potentials in Eq. (16), however, do not depend on k_z . Therefore, no ABS appears in a junction along the c -axis.
- ⁷³ There are two types of the zero-energy conductance peaks. One is a conductance peak which appears accidentally at zero-energy, the other is a conductance peak which should appear at the zero-energy because of, for example, the Andreev interface/surface bound state originating from the topology of the bulk wave functions. A zero-energy peak is not expected on the surface perpendicular to the c direction of Sr_2RuO_4 . Moreover, if the peak in Fig. 3a is caused by, for example, the Andreev bound states in F, the energy of the conductance peak is not affected by the details of a system such as the thickness. In Fig. 3a, the peaks at $\pm\Delta_0$ for $L = 0$ move in the $\mp E$ direction with increasing L . At $k_F L = 15$, these two peaks merge. For a longer L , the two peaks just pass each other.
- ⁷⁴ K. Yada, A. A. Golubov, Y. Tanaka, and S. Kashiwaya, Journal of the Physical Society of Japan **83**, 074706 (2014).
- ⁷⁵ K. Kawai, K. Yada, Y. Tanaka, Y. Asano, A. A. Golubov, and S. Kashiwaya, Phys. Rev. B **95**, 174518 (2017).
- ⁷⁶ M. Fogelström, D. Rainer, and J. A. Sauls, Phys. Rev. Lett. **79**, 281 (1997).
- ⁷⁷ Y. Tanaka, Y. Tanuma, K. Kuroki, and S. Kashiwaya, Journal of the Physical Society of Japan **71**, 2102 (2002).
- ⁷⁸ Y. Asano, Y. Tanaka, and S. Kashiwaya, Phys. Rev. B **69**, 134501 (2004).